A PRELIMINARIES

Markov Decision Process (MDP). A standard MDP can be represented as a tuple: $(\mathcal{S}, \mathcal{A}, \mathcal{P}, \mathcal{R}, \gamma, T)$, where $\mathcal{S}$ denotes the state set, $\mathcal{A}$ denotes an action set, $\mathcal{P}$ is the transition function: $\mathcal{S} \times \mathcal{A} \times \mathcal{S} \rightarrow [0, 1]$ and $\mathcal{R}$ is the reward function: $\mathcal{S} \times \mathcal{A} \rightarrow \mathbb{R}$. $\gamma \in [0, 1)$ is a discount factor and T is the decision horizon. The target of the agent is to optimize its policy to maximize the expected discounted cumulative reward.

Frameskip. Frame-skipping may be viewed as an instance of (partial) open-loop control, under which a predetermined sequence of (possibly different) actions is executed without heed to intermediate states. Aiming to minimize sensing, Kalyanakrishnan et al. (2021) proposes a framework for incorporating variable-length open-loop action sequences in regular (closed-loop) control. The primary challenge in general open-loop control is that the number of action sequences of some given length d is exponential in d. Consequently, the main focus in the area is on policies to prune corresponding data structures (Braylan et al., 2015). Since action repetition restricts itself to a set of actions with size linear in d, it allows for d itself to be set much higher in practice. With frame-skipping, the agent is only allowed to sense every d state: that is, if the agent has sensed a state s_t at time step $t >= 0$, it is oblivious to states$s_{t+1}, s_{t+2}, ..., s_{t+d-1}$, and next only observes s_{t+d}.

Variational Auto-encoder. The variational auto-encoder (VAE) is a directed graphical model with certain types of latent variables, such as Gaussian latent variables. A generative process of the VAE is as follows: a set of latent variable z is generated from the prior distribution $p_\theta(z)$ and the data x is generated by the generative distribution $p_\theta(x|z)$ conditioned on $z : z \sim p_\theta(z), x \sim p_\theta(x|z)$. In general, parameter estimation of directed graphical models is often challenging due to intractable posterior inference. However, the parameters of the VAE can be estimated efficiently in the stochastic gradient variational Bayes (SGVB) framework, where the variational lower bound of the log-likelihood is used as a surrogate objective function. In this framework, a proposal distribution $q_\theta(x|z)$, which is also known as a "recognition" model, is introduced to approximate the true posterior $p_\theta(x|z)$. The multilayer perceptrons (MLPs) are used to model the recognition and the generation models. Assuming Gaussian latent variables, the first term of Equation (2) can be marginalized, while the second term is not. Instead, the second term can be approximated by drawing samples $z^{(l)}(l = 1, ..., L)$ by the recognition distribution $q_\theta(x|z)$, and the empirical objective of the VAE with Gaussian latent variables is written as follows:

$$L_{VAE}(\phi, \psi) = \frac{1}{L} \sum_{\theta} (x|z^{(l)}) - KL\big(q_\phi(z|x)||N(0, I)\big) \tag{1}$$

B EXPERIMENTAL DETAILS

B.1 NETWORK STRUCTURE

Layer	Actor Network	Critic Network
Fully Connected	(state dim, 256)	(statedim + η dim + latent space dim, 128)
Activation	ReLU	ReLU
Fully Connected	(256, 128)	(256, 128)
Activation	ReLU	ReLU
Fully Connected	(128,latent space dim) and η dim	(128, 1)
Activation	Tanh	None

Table 1: Network Structures for DRL Methods

Our codes are implemented with Python 3.7.9 and Torch 1.7.1. All experiments were run on a single NVIDIA GeForce GTX 2080Ti GPU. Each single training trial ranges from 4 hours to 17 hours, depending on the algorithms and environments. For more details of our code refer to the HyAR.zip in the supplementary results. And will open source code in the near future.

Our codes are implemented with Python 3.7.9 and Torch 1.7.1. All experiments were run on a single NVIDIA GeForce GTX 2080Ti GPU. Each single training trial ranges from 4 hours to 17 hours, depending on the algorithms and environments. For more details of our code refer to the HyAR.zip in the supplementary results. And will open source code in the near future.

Our TD3 is implemented with reference to `github.com/sfujim/TD3` (TD3 source-code). DDPG and PPO are implemented with reference to `https://github.com/sweetice/Deep-reinforcement-learning-with-pytorch`. For a fair comparison, all the baseline methods have the same network structure (except for the specific components of each algorithm) as our MARS-TD3 implementation. As shown in Tab.1, we use a two-layer feed-forward neural

Model Component	layer	dimension
Conditional Encoder Network	Fully Connected (encoding)	$(\mathbb{R}^x, 256)$
	Fully Connected (condition)	(stae dim + η dim, 256)
	Element-wise Product	ReLU (encoding), ReLU(condition)
	Fully Connected	$(256, 256)$
	Activation	ReLU
	Fully Connected (mean)	(256, latent space dim)
	Activation	None
	Fully Connected (log std)	(256, latent space dim)
	Activation	None
Conditional Decoder, Prediction Network	Fully Connected (latent)	(latent space dim, 256)
	Fully Connected (condition)	(stae dim +η dim, 256)
	Element-wise Product	ReLU (encoding), ReLU(condition)
	Fully Connected	(256, 256)
	Activation	ReLU
	Fully Connected (η)	(256, action dynamic transition)
	Activation	None
	Fully Connected (reconstruction)	(256, multi-step action dim)
	Activation	None
	Fully Connected	$(256, 256)$
	Activation	ReLU
	Fully Connected (prediction)	(256, state dim)
	Activation	None

Table 2: Network structures for the Multi-step action representation (MARS).

network of 256 and 256 hidden units with ReLU activation (except for the output layer) for the actor network for all algorithms. For DDPG the critic denotes the Q-network. For PPO, the critic denotes the V-network. All algorithms (TD3, DDPG, PPO) output two heads at the last layer of the actor network, one for latent action and another for dynamic transition potential.

The structure of MARS is shown in Tab.2. We use element-wise product operation (Mahmood et al., 2018) and cascaded head structure (Fuchs et al., 2021) to our model.

B.2 HYPERPARAMETER

For all experiments, we use the raw state and reward from the environment, and no normalization or scaling is used. No regularization is used for the actor and the critic in all algorithms. An exploration noise sampled from N(0, 0.1) (Dong et al., 2009) is added to all baseline methods when selecting an action. The discounted factor is 0.99 and we use Adam Optimizer (Li et al., 2016) for all algorithms. Tab.3 shows the common hyperparameters of algorithms used in all our experiments.

Hyperparameter	TD3-frameskip	TD3-advance	MARS-PPO	MARS-TD3	MARS-DDPG	
Actor Learning Rate	$1e^{-4}$	$1e^{-4}$	$1e^{-4}$	$1e^{-4}$	$1e^{-4}$	$1e^{-4}$
Critic Learning Rate	$1e^{-3}$	$1e^{-3}$	$1e^{-3}$	$3e^{-4}$	$3e^{-4}$	$1e^{-3}$
Representation Model Learning Rate	None	None	None	$1e^{-4}$	$5e^{-3}$	$5e^{-3}$
Discount Factor	0.99	0.99	0.99	0.99	0.99	0.99
Batch Size	128	128	128	128	128	128
Buffer Size	$1e5$	$1e5$	$1e5$	$1e5$	$1e5$	$1e5$

Table 3: A comparison of common hyperparameter choices of algorithms. We use 'None' to denote the 'not applicable' situation.

B.3 ADDITIONAL IMPLEMENTATION DETAILS

For PPO, the actor network and the critic network are updated every 2 and 10 episode respectively for all environments. The clip range of the PPO algorithm is set to 0.2 and we use GAE (Sutton

& Barto, 2018) for a stable policy gradient. For DDPG, the actor network and the critic network is updated at every 1 environment step. For TD3, the critic network is updated every 1 environment step and the actor network is updated every 2 environment steps.

The default latent action dim is 8, We set the KL weight in representation loss L_{MARS} as 0.5. Environment dynamic prediction loss weight β is 5 (default).

C Additional Experiment

C.1 Generalization of MARS

We test MARS with popular RL methods on three tasks: Hopper, Walker, and hardMaze. To make the experiment fair, we used the same parameters for all methods and implemented them based on public code. We use each RL algorithm to train on three tasks under the ideal setting and compare them with their corresponding improvement methods. To show the optimal score after the algorithm convergence, we train all the algorithm's 2000000 time steps. The results in Tab.4 show that all methods can learn effective policies with the help of MARS and perform similarly to their ideal settings. The differences in scores are mainly due to the variation in performance of the RL algorithms. In summary, MARS can be combined with different methods to provide a reliable action space for solving FIMDP as normal MDP with RL.

Benchmarks	MARS-PPO	MARS-DDPG	MARS-TD3
Maze hard	256 | 0.7 ↑	243 | 2.5 ↑	311 | 16.3 ↑
Hopper	2811.4 | 73.5 ↓	1815.6 | 184.3 ↑	3384 | 53.1 ↑
Walker	3831.2 | 285.1 ↓	1032.7 | 201.9 ↓	4821.6 | 427.6 ↑

Table 4: MARS generalization verification. All tasks are set to constant FIMDP, interval is 8. The format of the data in the table is: MARS-RL score | the score gap. ↓ denotes score of MARS lower than the ideal setting baseline. ↑ denotes score of MARS higher than the ideal setting baseline. All scores are averaged over five runs.

C.2 Details of Ablation study

We conducted two experiments to show how well the two mechanisms of MARS work together. Although the results of randomized FIMDP and constant FIMDP are slightly different, the same conclusion can be derived: The green curves in Figure 1 demonstrate that the representation model with increased action transition scale is much better than the original VAE. This means that dynamic transition potential can create an action hidden space by explicitly modeling the dependence between multi-step actions. The blue curves also show that VAE with state dynamic prediction is better than the original VAE because it can represent action sequences that have similar environmental effects at close locations. Finally, the red curves show that the two mechanisms work well together in MARS, and combining them improves representation ability.

C.3 Validity verification of multiple interaction intervals

To further demonstrate the effectiveness of MARS in diverse fragmentary interaction scenarios. For constant fragmentary interaction control tasks, we uniformly set the forbidden interaction duration and conducted four experiments on Hopper. The results in Figure 2 show that MARS can solve most tasks effectively and still guarantee good scores at long intervals, but the effectiveness of MARS decreases significantly when the interval is too long (which is not common in real-world scenarios). We believe that this is because VAE is unable to effectively characterize excessively long sequences, leading to the failure of multi-step action space modeling.

In addition, to observe the sensitivity of MARS to interaction intervals on random FIMDP tasks, we uniformly set the forbidden interaction duration and conducted four experiments on Hopper. The results in Figure 3 show that in random FIMDP scenarios, MARS performs well in both short and medium-interval scenarios. However, convergence changes slowly in the very long interval scenario,

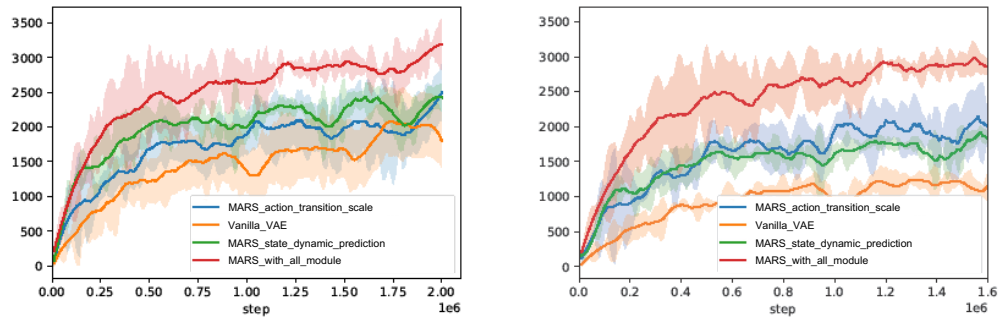

（a）Constant FIMDP　　（b）Random FIMDP

Figure 1: Details of ablation study. The curve and shade denote the mean and a standard deviation over 5 runs.

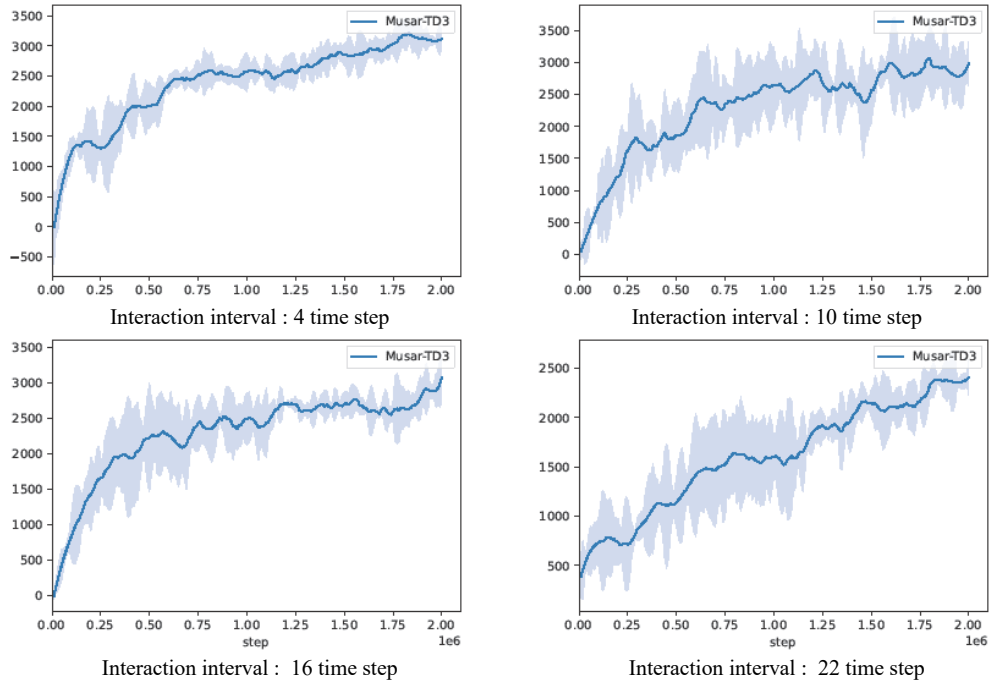

Interaction interval : 4 time step　　Interaction interval : 10 time step

Interaction interval : 16 time step　　Interaction interval : 22 time step

Figure 2: MARS's experimental results under four different settings of forbidden interaction duration. The curve and shade denote the mean and a standard deviation over 5 runs.

and the score is only half that of the medium interval task. Because MARS's representational capabilities are not perfect for modeling long action sequences for extremely long-spaced tasks (even if this setting rarely occurs in real-world scenarios). Therefore, in the future, we hope to find more suitable representation models to overcome this problem.

C.4 The influence of Latent action space dimension on algorithm effect

The representation space dimension of VAE is an important hyperparameter. If the latent space dimension is too low, a large amount of original data information will be lost, resulting in invalid representation space. On the contrary, when the latent space dimension is too large, the calculation

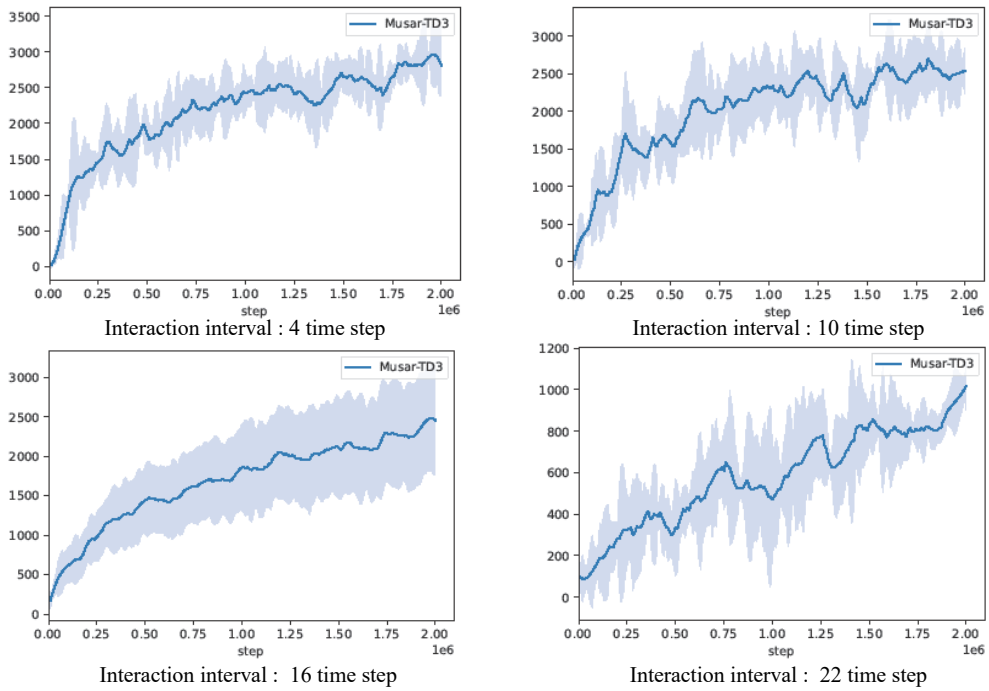

Figure 3: MARS's experimental results under four different settings of forbidden interaction duration. The curve and shade denote the mean and a standard deviation over 5 runs.

amount of the model will be increased. To verify the sensitivity of MARS to latent space dimensions, we test it on two tasks with different original action dimensions.

We set up four sets of latent space dimensions for constant FIMDP Hopper (interaction interval time step: 8, original action dimension: 3, so the action sequence dimension to be modeled is 24). The learning curve in Figure 4 shows that for raw data of such high dimensions, when the latent space dimension is set too low, the latent space information will be lost, resulting in the convergence failure of reinforcement learning policies. On the contrary, too high a latent space dimension increases the complexity of reinforcement learning policy exploration. In addition, we set up four comparison experiments on the 2dmaze task with a lower dimension of the original action sequence (interaction interval time step: 4, original action dimension: 2, so the action sequence dimension to be modeled is 8). The experimental results in Figure 5 show that the suboptimal policy can be learned when the latent space dimension is low, because the original data dimension is low. So the low-dimensional latent space loses less information. The score increases as the latent space dimension increases. However, when the latent space dimension is too high, the score will drop significantly, which is because of the exploration difficulties brought by high-dimensional latent space.

C.5 The influence of environment steps of warmup stage

In this section, we conduct some additional experimental results for a further study of MARS from different perspectives: We provide the exact number of samples used in the warm-up stage (i.e., stage 1 in Algorithm **??** in each environment in Tab.5. The number of warm-up environment steps is about $5\% \sim 10\%$ of the total environment steps in our original experiments. Moreover, we also conducted some experiments to further reduce the number of samples used in the warm-up stage (at most 80% off). See the colored results in Tab.5. MARS can achieve comparable performance with $< 3\%$ samples of the total environment steps.

Conclusion: The number of warm-up environment steps is about $5\% \sim 10\%$ of the total environment steps in our original experiments. The number of warmup environment steps can be further reduced

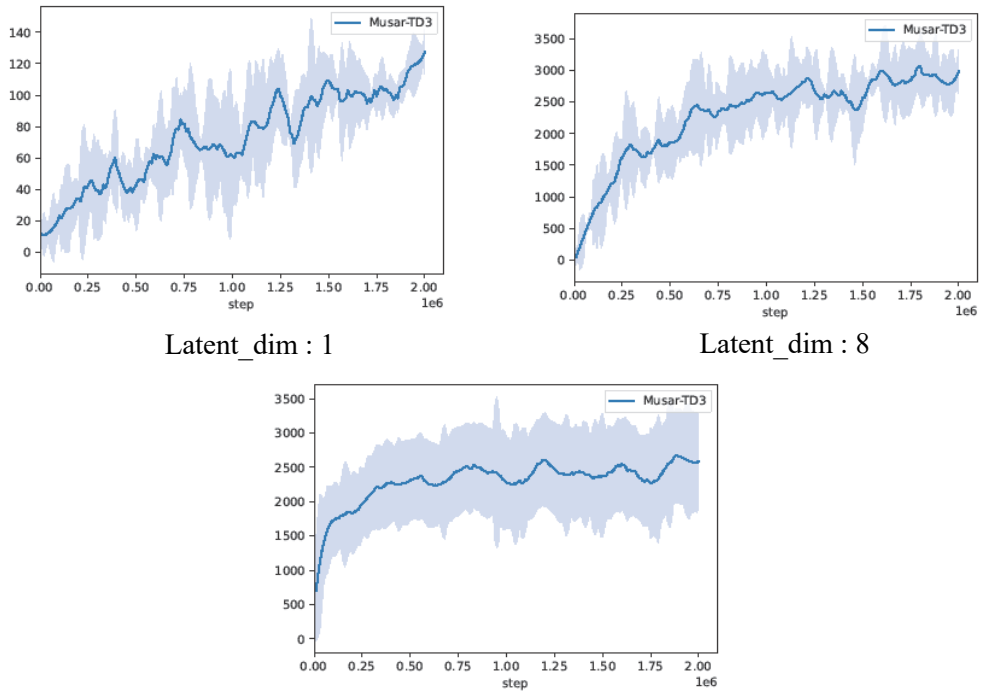

Figure 4: TD3 learning curves of three different latent space dimensions set the corresponding. The curve and shade denote the mean and a standard deviation over 5 runs.

by at most 80% off (thus leading to $< 3\%$ of the total environment steps) while the comparable performance of our algorithm remains.

Environment	Warm-up steps (original)	Warm-up steps (new)	Total Env. Steps
Hopper	400000(0.08|3219.1)	100000(0.02|3086.4)	5000000
Ant	400000(0.08|4305.7)	100000(0.02|4025.6)	5000000
Walker	400000(0.08|4961.3)	100000(0.02|4792.6)	5000000
HalfCheetah	400000(0.08|6593.2)	100000(0.02|6071.2)	5000000
2dmaze-medium	100000(0.083|127.8)	30000(0.025|118.5)	1200000
2dmaze-hard	100000(0.083|327.6)	35000(0.0292|296.1)	1200000

Table 5: The exact number of samples used in warm-up stage training in different environments. The column of 'original' denotes what is done in our experiments; the column of 'new' denotes additional experiments we conduct with fewer warm-up samples (and proportionally fewer warm-up training). For each entry $x(y|z)$, x is the number of samples (environment steps), y denotes the percentage number of $\frac{warm-up\ environment\ steps}{number\ of\ total\ environment\ steps\ during\ the\ training\ process}$, and z denotes the corresponding performance of MARS-TD3.

C.6 MARS-DDPG PSEUDOCODE

REFERENCES

Alexander Braylan, Mark Hollenbeck, Elliot Meyerson, and Risto Miikkulainen. Frame skip is a powerful parameter for learning to play atari. In *AAAI-15 Workshop on Learning for Gen-*

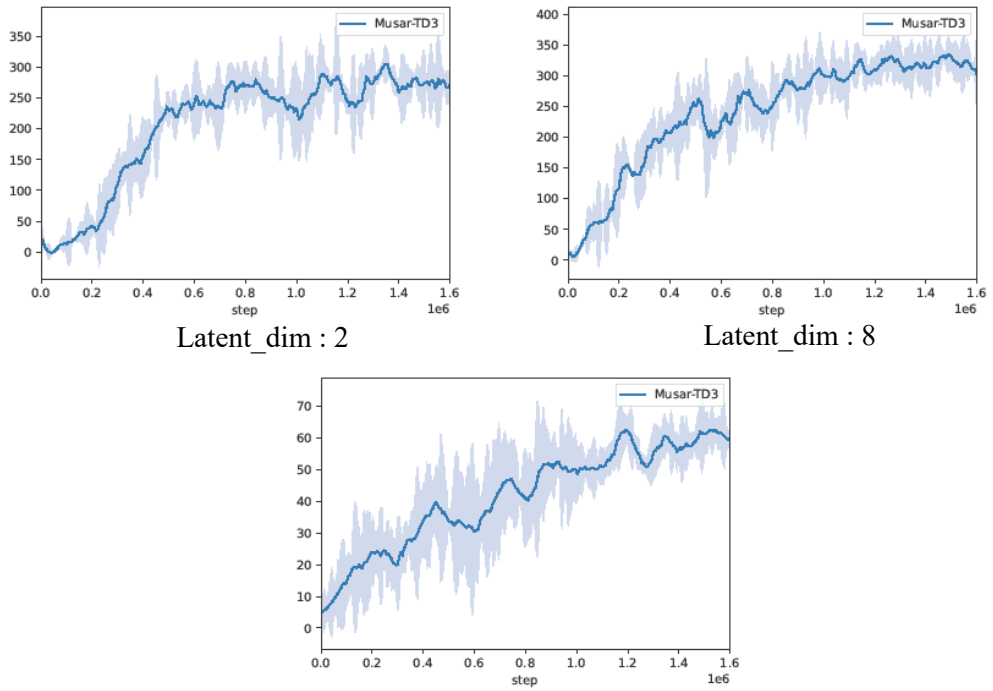

Figure 5: TD3 learning curves of three different latent space dimensions set the corresponding. The curve and shade denote the mean and a standard deviation over 5 runs.

Algorithm 1 MARS-DDPG

Initialize actor π_τ and critic networks Q_θ
Initialize conditional VAE q_ϕ, p_ψ and replay buffer D
Stage 1
while *not reaching warmup training times* **do**
Fill D with data generated by random policy or offline datasets
Update q_ϕ, p_ψ using samples in D
end while
Stage 2
while $t <$ *policy training time* **do**
$a_z, a_\eta = \pi_\tau$ (with Gaussian noise)
$u = p_\psi(a_z, a_\eta, s)$
Execute u, observe r and new state s'
Fill D with $(s, s_{t:t+c}, u, a_z, a_\eta, r, s')$
Sample from D, update Q_θ and pi_τ
if reach representation training time **then**Update q_ϕ, p_ψusing samples in D

eral Competency in Video Games, 2015. URL `http://nn.cs.utexas.edu/?braylan:aaai15ws`.

Xihua Dong, Xiaochen Li, and Dapeng Wu. Analysis of packet error probability in delay constrained communication over fading channels. In *2009 6th IEEE Consumer Communications and Networking Conference*, pp. 1–5. IEEE, 2009.

Florian Fuchs, Yunlong Song, Elia Kaufmann, Davide Scaramuzza, and Peter Dürr. Super-human performance in gran turismo sport using deep reinforcement learning. *IEEE Robotics and Automation Letters*, 6(3):4257–4264, 2021.

Shivaram Kalyanakrishnan, Siddharth Aravindan, Vishwajeet Bagdawat, Varun Bhatt, Harshith Goka, Archit Gupta, Kalpesh Krishna, and Vihari Piratla. An analysis of frame-skipping in reinforcement learning. *arXiv preprint arXiv:2102.03718*, 2021.

Yuliang Li, Rui Miao, Changhoon Kim, and Minlan Yu. Lossradar: Fast detection of lost packets in data center networks. In *Proceedings of the 12th International on Conference on Emerging Networking EXperiments and Technologies*, CoNEXT '16, pp. 481–495, New York, NY, USA, 2016. Association for Computing Machinery. ISBN 9781450342926. doi: 10.1145/2999572.2999609. URL https://doi.org/10.1145/2999572.2999609.

A Rupam Mahmood, Dmytro Korenkevych, Brent J Komer, and James Bergstra. Setting up a reinforcement learning task with a real-world robot. In *2018 IEEE/RSJ International Conference on Intelligent Robots and Systems (IROS)*, pp. 4635–4640. IEEE, 2018.

Richard S. Sutton and Andrew G. Barto. *Reinforcement Learning: An Introduction*. A Bradford Book, Cambridge, MA, USA, 2018. ISBN 0262039249.